Experimental study of non-Darcy flow characteristics in permeable stones

Zhongxia Li[1], Junwei Wan[1], Tao Xiong[1], Hongbin Zhan[2]*, Linqing He[3], Kun Huang[1]*

[1]School of Environmental Studies, China University of Geosciences, 430074 Wuhan, China.

[2]Department of Geology and Geophysics, Texas A & M University, College Station, TX 77843-3115, USA.

[3]Changjiang Institute of Survey Technical Research MWR, Wuhan, China.

* *Correspondence to*:

Dr. Hongbin Zhan (zhan@tamu.edu);

Dr. Kun Huang (cugdr_huang@cug.edu.cn).

Abstract.

This study provides experimental evidence of Forchheimer flow and transition between different flow regimes from the perspective of pore size of permeable stone. We have firstly carried out the seepage experiments on four kinds of permeable stones with sizes of 24, 46, 60 and 80 mesh size, respectively, which corresponding to mean particle sizes (50% by weight) of 0.71 mm, 0.36 mm, 0.25 mm, and 0.18 mm. The seepage experiments show that obvious deviation from Darcy flow regime is visible. In addition, the critical specific discharge corresponding to the transition of flow regimes (from pre-Darcy to post-Darcy) increases with the increase of particle sizes. When the “pseudo” hydraulic conductivity (*K*) (which is computed by the ratio of specific discharge (*q*) and hydraulic gradient) increases with the increase of *q*, the flow regime is denoted as the pre-Darcy flow. After *q* increases to a certain value, the “pseudo” hydraulic conductivity begins to decrease, this regime is called the post-Darcy flow. In addition, we use the mercury injection technique to measure the pore size distribution of four permeable stones with different particle sizes. The mercury injection curve is divided into three stages. The beginning and end segments of the mercury injection curve are very gentle with relatively small slopes, while the intermediate mercury injection curve is steep, indicating that the pore size in permeable stones is relatively uniform. The porosity decreases as the mean particle sizes increases. The mean pore size can faithfully reflect the influence of particle diameter, sorting degree and arrangement mode of porous medium on seepage parameters. This study shows that the size of pores is an essential factor for determining the flow regimes. In addition, the Forchheimer coefficients are also discussed in which the coefficient *A* (which is related to the linear term of the Forchheimer equation) is linearly related to $1/d^2$ as $A = 0.0025\left(1/d^2\right) + 0.003$; while the coefficient *B* (which is related to the quadratic term of the Forchheimer equation) is a quadratic function of $1/d$ as $B = 1.14\times10^{-6}\left(1/d\right)^2 - 1.26\times10^{-6}\left(1/d\right)$. The porosity (*n*) can be used to reveal the effect of sorting degree and arrangement on seepage coefficient. A larger porosity leads to smaller coefficients A and B under the condition of the same particle size.

Keywords**:** permeable stone, mercury injection technique, pore size, flow regime, non-Darcy flow.

1. Introduction

Darcy (1857) conducted a steady-state flow experiment in porous media and concluded that specific discharge was proportional to hydraulic gradient, which is the Darcy's law described as follow:

$$q = KJ \tag{1}$$

where q is the specific discharge, J is the hydraulic gradient, K is the hydraulic conductivity. However, when the specific discharge increases above a certain threshold, deviation from Darcy's law is evident and the flow regime changes from Darcy flow regime to the so called non-Darcy flow regime (Bear, 1972), which was first observed by Forchheimer (1901), who proposed a widely used non-Darcy flow equation (the Forchheimer equation) as follow:

$$J = Aq + Bq^2 \tag{2}$$

where A and B are constants related to fluid properties and pore structure. The first and second terms on the right side of Eq. (2) more or less reflect the contributions of viscous and inertial forces (or resistance to flow), respectively.

From the Forchheimer equation, we can see that when the specific discharge is sufficiently small, the inertial force can be ignored, the equation is transformed to the form of Darcy's law. On the other hand, when the specific discharge is sufficiently large, the viscous force can be ignored, the equation is transformed to the fully developed turbulent flow.

In addition to the polynomial function such as the Forchheimer equation, there are also several power-law functions proposed to describe the non-Darcy flow, one of the most commonly used power-law equations is the Izbash equation (Izbash, 1931), which is written as:

$$J = aq^b \tag{3}$$

where a and b are the empirical parameters that depend on flow and materials properties, the coefficient b is usually between 1 and 2.

Because of its applicability for a wide range of velocity spectrum and its sound physics, many scholars have adopted the Forchheimer equation (among many different types of equations) to explore the non-Darcy flow. Besides, the theoretical background of the Forchheimer equation has been discussed in details (Panfilov and Fourar, 2006). Numerous experimental data have confirmed the validity of the Forchheimer equation for a variety of nonlinear flow phenomena (Geertsma, 1974; Scheidegger, 1957; Wright, 1968). The quadratic Forchheimer law has also been revealed as a result of numerical modelling by simulating the Navier–Stokes flow in corrugated channels (Koch and Ladd, 1996; Skjetne et al., 1999; Souto and Moyne, 1997). To sum up, the Forchheimer equation will be selected as a representative to describe non-Darcy flow in this study.

Since the transition between Darcy flow and non-Darcy flow is important and difficult to quantify, different scholars have carried out experiments using a wide range of porous media, including homogeneous and heterogeneous porous media. Most of the experimental studies have focused on the influence of mean particle size on flow state transition using homogeneous porous media. In fact, it was believed that the nonlinear (or non-Darcy) flow behavior in porous media was due to turbulent effect of flow in earlier studies and the Reynold number (Re) was widely used to quantify the initiation of non-Darcy flow. Bear (1972) concluded that the critical Re (denoted as Re_c) of flow states (or the Re value at which flow starts to change from Darcy flow regime to non-Darcy flow regime) is between 1 to 10. This finding was based on experimental data collected in packed sand beds (Ergun, 1952; Fancher and Lewis, 1933; Lindquist, 1933; Scheidegger, 1960). Schneebeli (1955) and Wright (1968) experimentally measured the value of *Re* at the beginning of turbulence and concluded that at very high velocities, the deviation from Darcy's law is due to inertial effects followed by turbulent effects. In addition, Dudgeon (1966) confirmed that Re_c is about 60~150 for relatively coarse particle medium including river gravels, crushed rock particles and glass marbles with grain sizes from 16 mm to 152 mm. Dudgeon (1966) indicated that the deviation from Darcy's law was not entirely due to turbulence, but in a large extent due to inertial forces. Besides, Geertsma (1974) proposed an empirical relationship among the inertial coefficient, permeability and porosity by conducting non-Darcy flow experiments in unconsolidated and consolidated sands. The laser anemometry and flow visualization studies of fluid flow in porous structures were used by Dybbs and Edwards (1984), they observed the nonlinear behavior at Reynolds numbers around 150. Latifi et al. (1989) found that the transition from unsteady-state laminar flow to non-Darcy flow in packed beds of spheres was between *Re* values of 110 and 370. Seguin et al. (1998) investigated the characterization of flow regimes in various porous media with electrochemical techniques and found that the end of the Darcy flow regime in packed beds of particles appeared at *Re* about 180. Besides, Bu et al. (2014) indicated that the Darcy flow in the packed beds would end at *Re* around 100 by using electrochemical techniques. Sedghi-Asl et al. (2014) found that the Darcy's law was usually not valid for rounded particle sizes greater than 2.8 mm, according to the experimental results of flow in different sizes of rounded aggregates. Our previous experimental research (Li et al., 2017) indicated that when the particle size was smaller than 2.8 mm, the flow state gradually changed from the pre-Darcy flow to the post-Darcy flow when the specific discharge increased. When the medium particle sizes get even larger, such as 4.5 mm, 6.39 mm, 12.84 mm, and 16 mm (Moutsopoulos et al., 2009), only the post-Darcy flow exists. Based on above analysis, we can see that many previous experiments were carried out on homogeneous porous media, the non-Darcy flow characteristics are quite different in porous media with various particle sizes.

Among the numerous experimental studies reviewed above on transition of Darcy flow to non-Darcy flow, it is evident that most of them focused on the effect of the mean particle size rather than the particle size distribution. Recently, a few investigators recognized the importance of particle size heterogeneity in understanding the transition of flow regimes, and have carried out a series of experiments to address the issue. For instance, Van Lopik et al. (2017) provided new experimental data on nonlinear flow behavior in various uniformly graded granular material for 20 samples, ranging from medium sands (d_{50} > 0.39 mm) to gravel (d_{50} >6.34 mm). In addition, they investigated the nonlinear flow behavior through packed beds of five different types of natural sand and gravel from unconsolidated aquifers, as well as 13 different composite mixtures of uniformly graded filter sands at different grain size distributions and porosity values (Van Lopik et al., 2019). We have also discussed the effect of particle size distribution on Forchheimer flow and transition of flow regimes in a previous study (Li et al., 2019b). Our previous study showed that the uniformity coefficient of porous media (a term used to describe the pore size distribution) is a critical factor for determining the flow regimes besides the mean particle sizes. Yang et al. (2019) investigated the effects of the particle size distribution on the seepage behavior of a sand particle mixture and evaluated the validity of empirical formulas of permeability and inertia factor used in engineering practice. Shi et al. (2020) discussed the non-Darcy flow behavior of granular limestone with a wide range of porosity from 0.242 to 0.449. Based on the experimental data, Shi et al. (2020) proposed an empirical hydraulic conductivity-porosity relation as well as an expression of inertial coefficient. Regardless of the media investigated are homogeneous or heterogeneous, the essence of the water passing capacity of porous media is pore sizes. Thus, exploring the distribution of pores in porous media is the basis of studying flow dynamics of Darcy and non-Darcy flows.

The purpose of this study is to provide a quantitative analysis on the effects of pore size on the transition of flow regimes between Darcy and non-Darcy flows based on a series of laboratory experiments. To meet the objectives, we have firstly carried out the seepage experiments of permeable stones with four different particle sizes. After that, we have conducted mercury injection experiments on permeable stones with four different particle sizes, the pore size distributions with different particle sizes are obtained. Finally, the effect of pore size on the transition of flow regimes and Forchheimer coefficients are discussed based on the experimental results.

2. Experimental methodology

2.1 Experimental setup and methods

The experimental device is mainly composed of three parts: a water supply device, a seepage experimental device and a measuring device. The schematic diagram of the experimental apparatus is shown in Fig. 1. The water supply device consists of a tank, a centrifugal pump and a flow regulating valve. The seepage experimental device consists of a permeable stone and a plexiglass column. The measurement device monitors the real-time water temperature and pressure. The water temperature is measured using a thermometer with a precision of measurement of 0.1 °C. The water-level fluctuation is measured to calculate the flow rate by a pressure transducer (CY201, Chengdu test LLC, China) in the range of 0–20 kPa with ±0.1% accuracy. The measuring device consists of a cylindrical tank and a pressure transducer. The sample of permeable stone is 60 mm in length with a circular cross section of 51.3 mm in diameter. Two pressure transducers are set at the entrance and exit of the column to measure the pressure drop. To minimize the boundary effects, the pressure transducer is placed 30 mm away from either end of the column, the way of pressure measurement is consistent with our previous studies (Li et al., 2017; Li et al., 2019b).

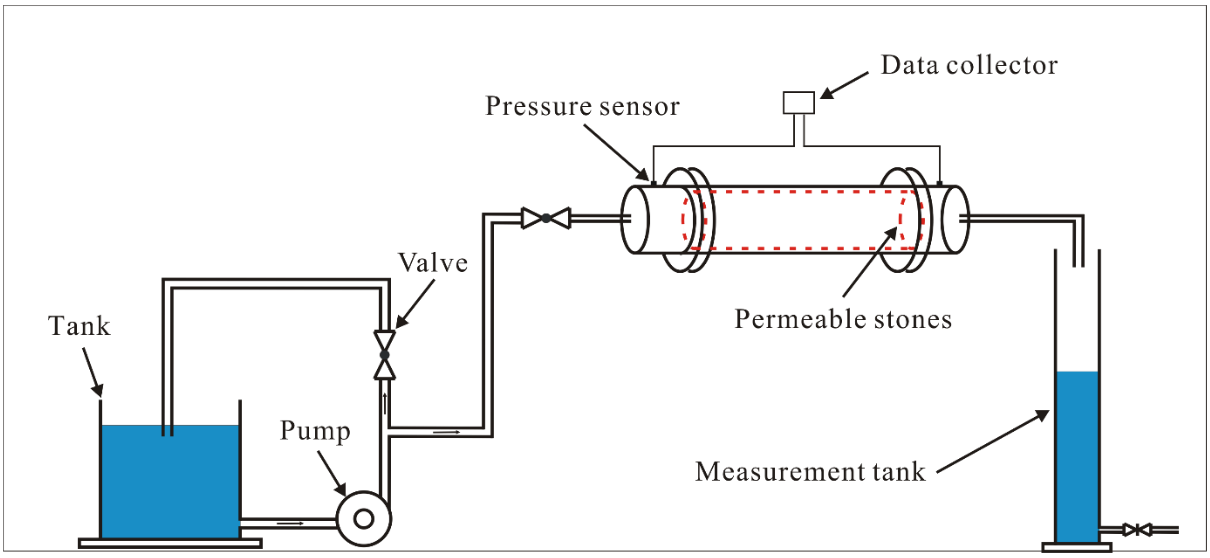

Figure 1. The schematic diagram of experimental apparatus.

2.2 Experimental Materials and Procedures

Four different particle sizes of permeable stones are selected to carry out the seepage experiment in this study. It is necessary to make a brief overview of the preparation process of permeable stone, which is a type of artificially made tight porous medium formed by sand grains and cementing compound. In the process of preparing permeable stones, a certain particle size of sand and cementing compound is put in a mold, which is consolidated at room temperature. The permeable stone is widely used in daily life. At present, the most commonly used permeable base materials in urban road construction, “sponge” city construction and ecological restoration research are large-pore cement stabilized gravel, large-diameter permeable asphalt mixture and so on (Guan et al., 2021; Li et al., 2019a; Suo et al., 2021; Yu et al., 2021). The discharge capacity of various permeable stones is different. However, the increase of pore space will lead to the decrease of pavement performance and mechanical strength (Han et al., 2016; Wang et al., 2021). Therefore, many scholars have carried out a lot of research on controlling the proper pore space of permeable stone (Alvarez et al., 2010;

Prowell et al., 2002; Xie and Watson, 2004).

We have carried out the seepage experiments on four kinds of permeable stones with different sizes of 24, 46, 60 and 80 mesh size, where the mesh size is defined as the number of mesh elements (all in square shapes) in a one inch by one inch square, which means that a greater number of mesh size implies a smaller particle size. For instance, we can convert above four different mesh sizes of permeable stones into corresponding particle sizes of 0.71 mm, 0.36 mm, 0.25 mm and 0.18 mm, respectively. In respect to pore composition, the pore distribution is concentrated over a narrow pore size range, the proportion of large pores and small pores is very small. The average particle size can reflect the overall permeability of the porous media. The pore structure of permeable rock will not change in the process of the seepage experiment under room temperature, the physical diagrams of four kinds of permeable stones with different particle sizes are shown in Fig. 2 and Fig. 3.

Figure 2. Physical drawing of permeable stones with four different particle sizes.

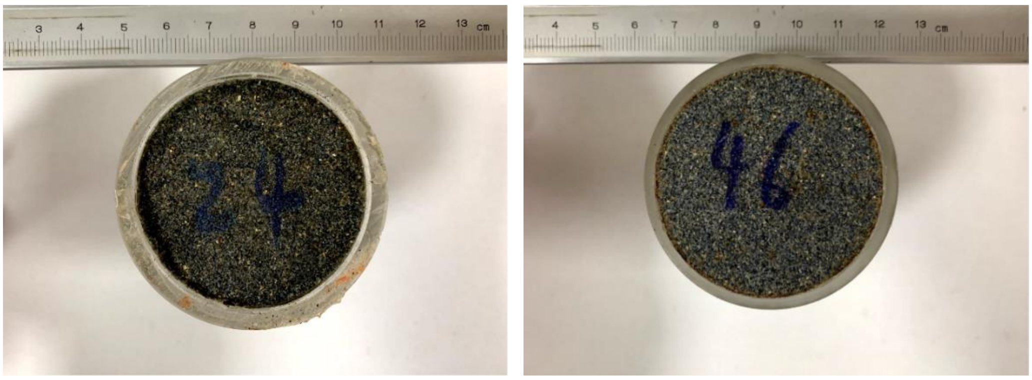

(a) (b)

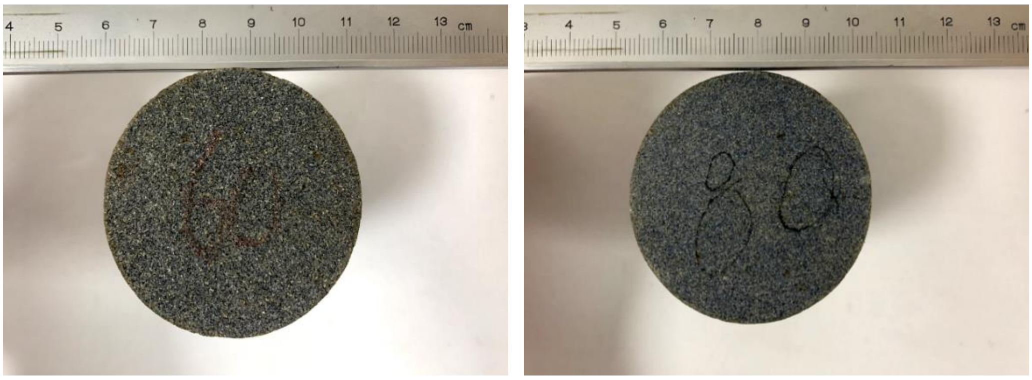

(c) (d)

Figure 3. Permeable stones with different particle sizes: (a) 24 mesh size or 0.71 mm, (b) 46 mesh size or 0.36 mm, (c) 60 mesh size or 0.25 mm, and (d) 80 mesh size or 0.18 mm.

It is worth mentioning that the contact surface of the sample and the plexiglass column is sealed to prevent any preferential flow through the wall of the plexiglass column. After the permeable stone is inserted into the plexiglass column, both ends are sealed with silicone glue. Water passing through the permeable stone is then collected by a cylindrical tank. Moreover, the ratio of the internal diameter of the column to the particle size of permeable stone is greater than 12, which can eliminate any possible wall effect on the seepage according to Beavers et al. (1972). When carrying out the experiment, it usually takes about two hours to saturate the permeable stone. For each packed sample, more than 25 tests with different constant inlet pressures were conducted under steady-state flow condition. In addition, for each group of permeable stone, repeated tests under the same experimental condition were carried out 3-4 times to ensure the accuracy of the results.

3. Results and discussion

3.1 Permeable stone seepage experiment

In this study, the mean particle size is corresponding to 50% by weight hereinafter. Such a definition of mean particle size may be different from some other studies such as Fetter (2001) which has used 10% by weight as the mean particle size. The relationship between the specific discharge (q) and the hydraulic gradient (J) of permeable stones is plotted in Fig. 4. The units of specific discharge mentioned in this study are all converted to meters per day (md^{-1}). Therefore, the best-fitting exercise yields Forchheimer numbers with orders of magnitudes to be about -4. In addition, the critical Forchheimer numbers proposed by Zeng and Grigg (2006) and Javadi et al. (2014) are empirical. In fact, the transition between Darcy to non-Darcy is successional over a certain range of Forchheimer numbers. The non-Darcy flow criterion applicable to different pore media is established by conducting seepage resistance experiments in homogeneous and heterogeneous porous media in our previous study (Li et al., 2017; Li et al., 2019b), which is consistent with the results of Zeng and Grigg (2006). Generally speaking, the q-J and q-K curves are the most commonly used methods to analyze flow regime when conducting seepage resistance experiments in porous media. However, the nonlinear characteristics of q-J curve are not obvious due to the relatively small velocity range used in the experiments. The traditional hydraulic conductivity is the ratio of the specific discharge versus the hydraulic gradient (q/J), it is a constant if Darcy's law is applicable, which is denoted as K_D (Li et al., 2019b). In fact, the ratio of q/J is no longer a constant for the problems discussed in this study. In a word, the q-K curve can be used to observe the transition of flow state more intuitively.

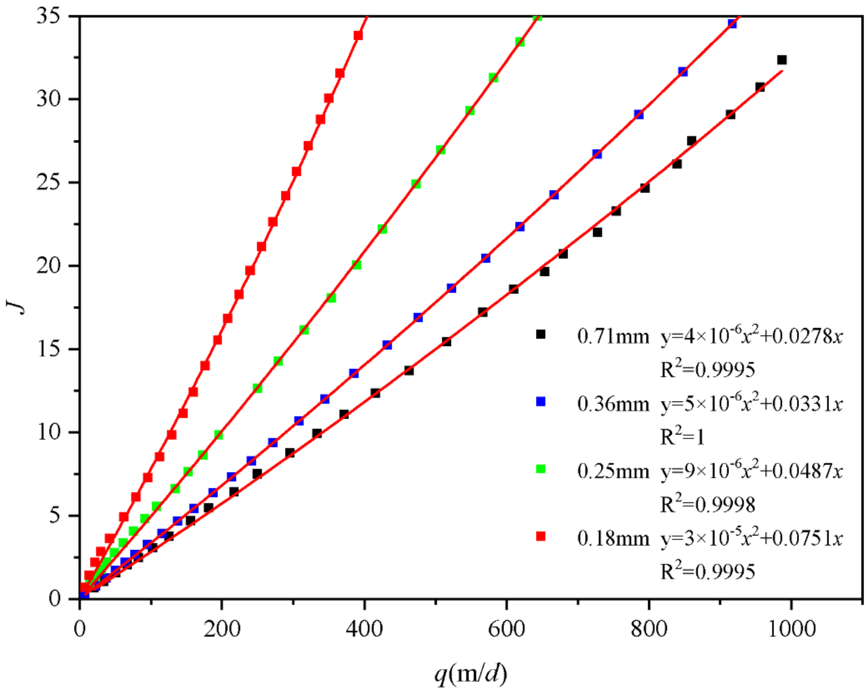

Figure 4. Variation of J with q of four permeable stones with different particle sizes.

Fig. 4 shows that when q is somewhat the same, a larger mesh size (which means a smaller particle size) will lead to a larger J. The results are consistent with our previous studies (Huang et al., 2013; Li et al., 2017; Li et al., 2019b). However, the nonlinear characteristics of q-J curve are not obvious due to the relatively small velocity range used in the experiments. Nevertheless, the best-fitting results using the Forchheimer equation are satisfactory. To analyze the influence of pore size on seepage flow regimes, we have obtained the relationship between q and the "pseudo" hydraulic conductivity (K) (which is computed using q/J) of four permeable stones with different particle sizes, as shown in Fig. 5. We should point out that the "pseudo" hydraulic conductivity term discussed here for non-Darcy flow is usually not a constant, thus it is different from the hydraulic conductivity term used in Darcy's law, which is a constant. It is obvious that the hydraulic conductivity is not a constant with the increase of specific discharge, so it is called the "pseudo" hydraulic conductivity (Li et al., 2019b).

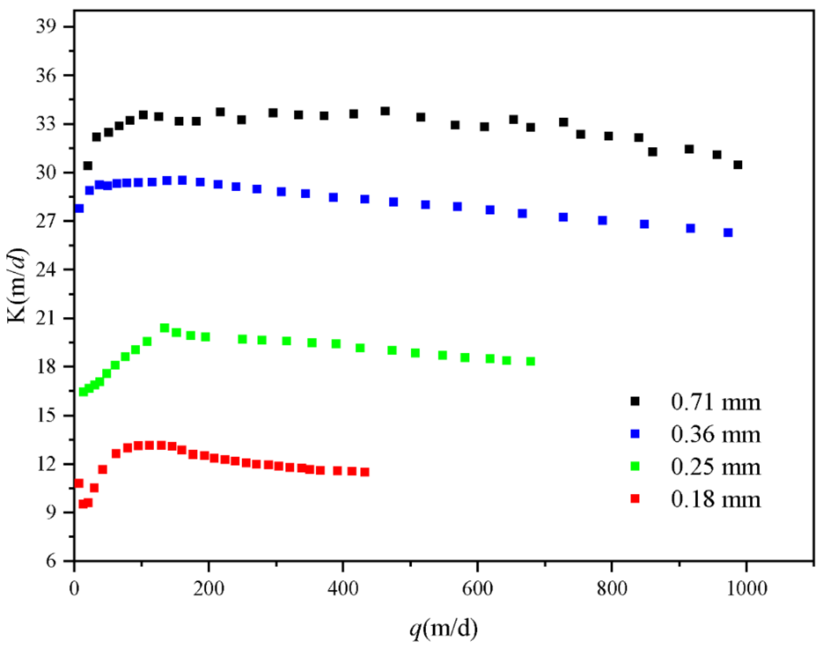

Figure 5. Variation of K with q of four permeable stones with different particle sizes.

We can divide the q-K curve into two segments: for the first segment, K increases with the increase of q, which is denoted as the pre-Darcy flow. For the second segment, after q increases to a certain value, K begins to decrease with q, which is called the post-Darcy flow. In fact, Izbash (1931) presented the equation as $q = M\left(\frac{dH}{dx}\right)^m = Mi^m$, where M and m are the coefficients determined by fluid flow and properties of porous media. When m=1, the Izbash equation reduces to Darcy law, when m>1, the Izbash equation corresponds to the pre-Darcy flow and when m<1, the Izbash equation refers to the post-Darcy flow (Dejam et al., 2017; Soni et al., 1978). Besides, Dejam et al. (2017) carried out a more detailed study on issues related to the pre-Darcy and post-Darcy flows. The influence of pre-Darcy flow on the pressure diffusion for homogenous porous media is studied in terms of the nonlinear exponent and the threshold pressure gradient. When the hydraulic gradient is small (and q is small as well), a great portion of water is bounded (or becomes immobile) on the surface of solids due to the solid-liquid interfacial force, only a small fraction of the water is mobile and free to flow through the pores. In addition, another justification for the pre-Darcy behavior may be due to an effect of a stream potential which generates small countercurrents along pore walls in a direction against the main flow (Bear, 1972; Scheidegger, 2020). Swartzendruber (1962b) stated that the surface forces arose in a solid-fluid interface due to strong negative charges on clay particle surfaces, and the dipolar nature of water molecules caused a pressure gradient response to be nonlinear and led to the pre-Darcy flow (Swartzendruber, 1962a). As the hydraulic gradient increases (and q increases as well), the initial threshold for mobilizing the previously immobile water near the solid-liquid surface is overcome and more water participates in flow. For this reason, the "pseudo" hydraulic conductivity increases with the increase of hydraulic gradient and the specific discharge in the first segment. When the specific discharge increases to the critical specific discharge (q_c), the "pseudo" hydraulic conductivity is maximized. According to $K=\frac{q}{Aq+Bq^2}=\frac{1}{A+Bq}$ based on Eq. (2), we can find that the "pseudo" hydraulic conductivity begins to decrease as the specific discharge continues to increase. Besides, the critical specific discharge corresponding to the transition of flow regimes (from pre-Darcy to post-Darcy) increases with the increase of particle sizes (or decrease of mesh sizes).

3.2 Mercury injection experiment

The particle size, different grain size distributions and degree of sorting are the main factors that determine the size and shape of pores. The shape of the pores determines the tortuosity and distribution of flow paths, which are related to viscous and inertial flow resistances. It is generally accepted in previous studies that the pore sizes of porous media have an impact on the seepage law (Maalal et al., 2021; Zhou et al., 2019). However, the structure of natural porous media is very complex, and it is difficult to quantify the effects of the arrangement of particles on the seepage law. The characteristics of pore size distribution contains critical information for quantifying the flow regimes. The mercury intrusion porosimetry and the nitrogen adsorption isotherm are two commonly used methods to characterize the pore sizes and their distribution (Rijfkogel et al., 2019). Besides, other techniques can also be used to derive the pore size distribution, such as small-angle neutron and X-ray scattering measurements, CT images and nuclear magnetic resonance (Anovitz and Cole, 2015; Hall et al., 1986; Kate and Gokhale, 2006; Lindquist et al., 2000). In this study we will use the mercury injection technique to measure the pore size distribution of the four permeable stones with different particle sizes and use the information to describe the flow regimes.

To quantitatively study the pore size and pore throat distribution, we need to envisage a physically based conceptual model to describe the pore structures of permeable stones. The commonly used model is the so-called capillary model (Pittman, 1992; Rezaee et al., 2012; Schmitt et al., 2013), which approximates the connected pores as many paralleled capillaries. The capillary forces are generated at the phase interface due to the surface tension between the solid and liquid phases when liquid flows in a capillary. The capillary force is directed toward the concave liquid level, it is shown as (Washburn, 1921):

$$P_c = \frac{2\sigma\cos\theta}{r} \tag{4}$$

where P_c is the capillary force, σ is the solid-liquid interfacial tension, θ is the wet angle between the liquid and the solid surface, r is the radius of curvature in capillary.

Since mercury is a nonwetting phase to solids, so to get mercury into the pores of the permeable stone, an external force (or displacement pressure) must be applied to overcome the capillary force. When a greater pressure is applied, mercury can enter smaller pores. When a certain pressure is applied, the injection pressure is equivalent to the capillary pressure in the corresponding pore. Then we can calculate the corresponding capillary radius according to Eq. (4), the volume of mercury injected is the pore volume.

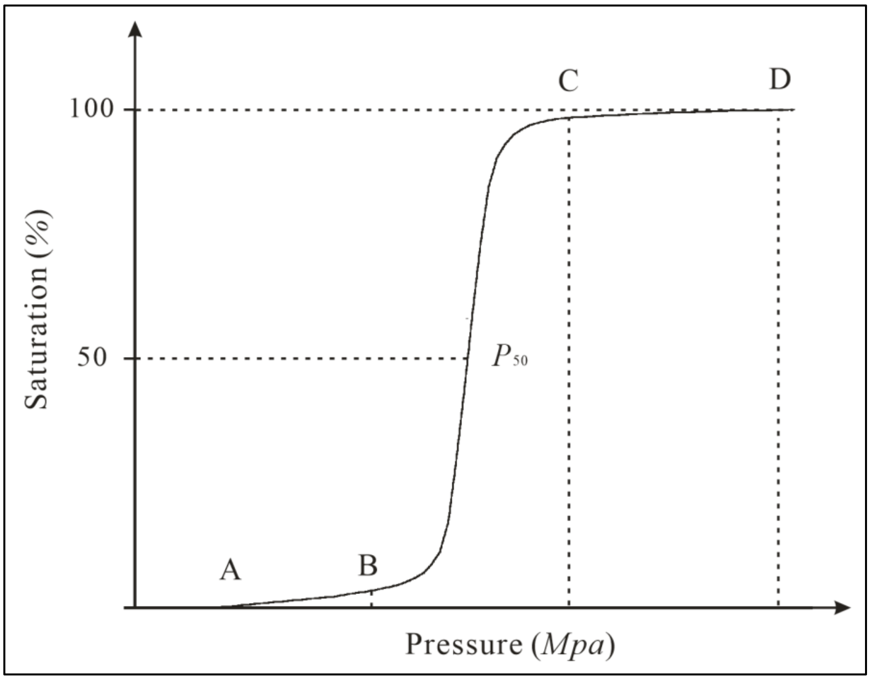

Figure 6. Schematic diagram of pressure changes with saturation: the initial stage (A-B), the intermediate mercury entry stage (B-C), and the end stage (C-D).

By continuously increasing the injection pressure, one can obtain the curve of injection pressure and the volume of injected mercury, from which one can also obtain the pore-throat distribution curve and capillary pressure curve. According to the amount of mercury injected at different injection pressures, the relation between the injection pressure and the injection saturation is shown in Fig. 6.

Fig. 6 shows that the mercury injection curve can be divided into three stages. Firstly, during the initial stage (A-B) which has a very mild slope, the intake pressure is very small and the intake saturation is also very low. With the increasing of the injection pressure, the intake saturation slowly increases. Secondly, during the intermediate mercury entry stage (B-C) which has a steep slope, a small pressure change will lead to a significant saturation change. This means that the pores are relatively uniform and the differences in pore sizes are small. It is well known that for mercury injection experiments, as injection pressure increases, the injection saturation will gradually increase and eventually all the pores will be filled with mercury. As can be seen from Fig. 7, with the continuous injection of mercury, the pressure of permeable stones with different particle sizes varies with saturation, which is reflected in the different pressures P_B and P_C at different stages. However, the reason for observing the different pressures is the difference of pore size distribution in the permeable stones. Therefore, the pressure ratio of B and C (P_C/P_B) can be used as one of the criteria to characterize the heterogeneity of pore size in porous media. Besides, when the saturation reaches 50%, the corresponding pressure value (P_{50}) reflects the characteristics of the mean pore size, a larger P_{50} leads to a larger mean pore size. Finally, during the end stage (C-D) which has a very mild slope as well, the amount of mercury will not increase considerably when the injection pressure increases. This indicates that nearly all the pores are essentially filled with mercury, then the mercury injection experiment is completed. After completing the mercury injection experiments, we have obtained the mercury injection curves of four permeable stones with different particle sizes, as shown in Fig. 7.

We can make a number of interesting observations based on Fig. 7. Firstly, the pressure at the starting point (when the saturation begins to increase), denoted as P_{A}, increases as the mean particle size decreases. This means that the maximum pore size in permeable stone decreases with the decrease of the mean particle sizes. Secondly, the mercury injection curves of four permeable stones all include steep intermediate stages, indicating that the pore size distributions are all relatively uniform. The corresponding pressure values at points B and C increase as the mean particle sizes decreases. Moreover, the pressure ratios corresponding to points B and C (P_C/P_B) also decrease with the decrease of particle sizes, suggesting even more uniform pore size distributions with decreasing particle sizes. Thirdly, the intermediate mercury entry stages gradually shift to the right with the decrease of particle sizes. When the saturation reaches 50%, the corresponding pressure (the median pressure) decreases with the increase of the mean particle sizes. Fourthly, the mercury injection curves of these four permeable stones with different particle sizes all approach 100% saturation with very mild slopes, indicating that there are few small pores in the permeable stones. We have extracted the key pressure characteristic values of mercury injection experiment of Fig. 7, and listed the results in Table 1.

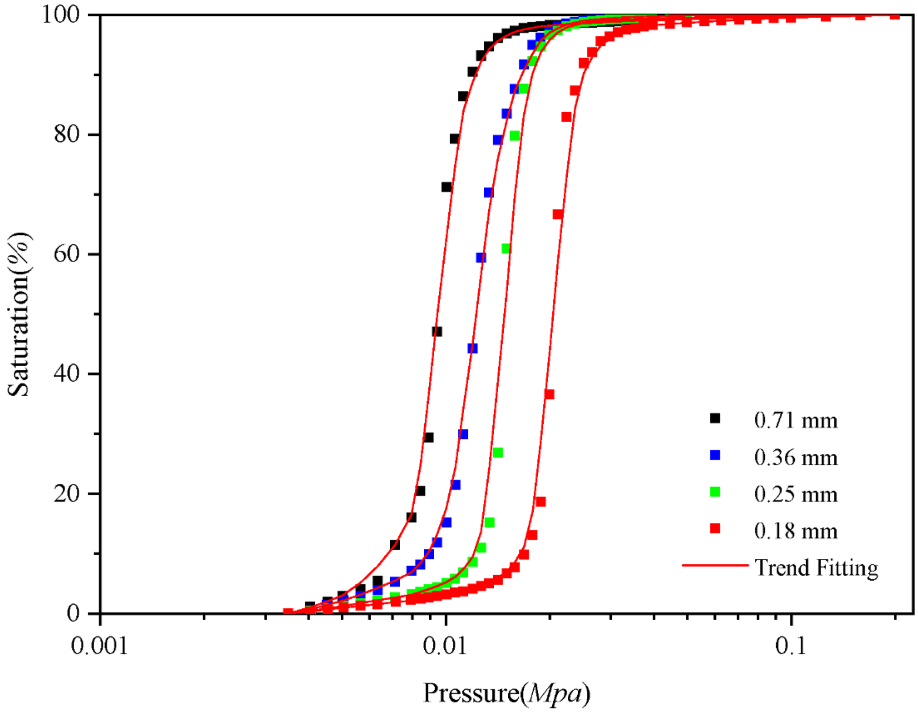

Figure 7. Variation of pressure with saturation of four permeable stones with different particle sizes.

Table 1. Pressure characteristic values of four permeable stones with different particle sizes.

Mesh size	$P_A(MPa)$	$P_B(MPa)$	$P_C(MPa)$	$P_{50}(MPa)$	P_C/P_B
24	0.0041	0.0064	0.0133	0.0094	2.0987
46	0.0045	0.0071	0.0188	0.0119	2.6374
60	0.0051	0.0112	0.0211	0.0150	1.8764
80	0.0057	0.0158	0.0281	0.0211	1.7758

To observe the pore size distributions of the four permeable stones with different particle sizes in more details, we can calculate the percentages of different pore sizes in permeable stones according to the mercury injection curves, as shown in Figs. 8-11.

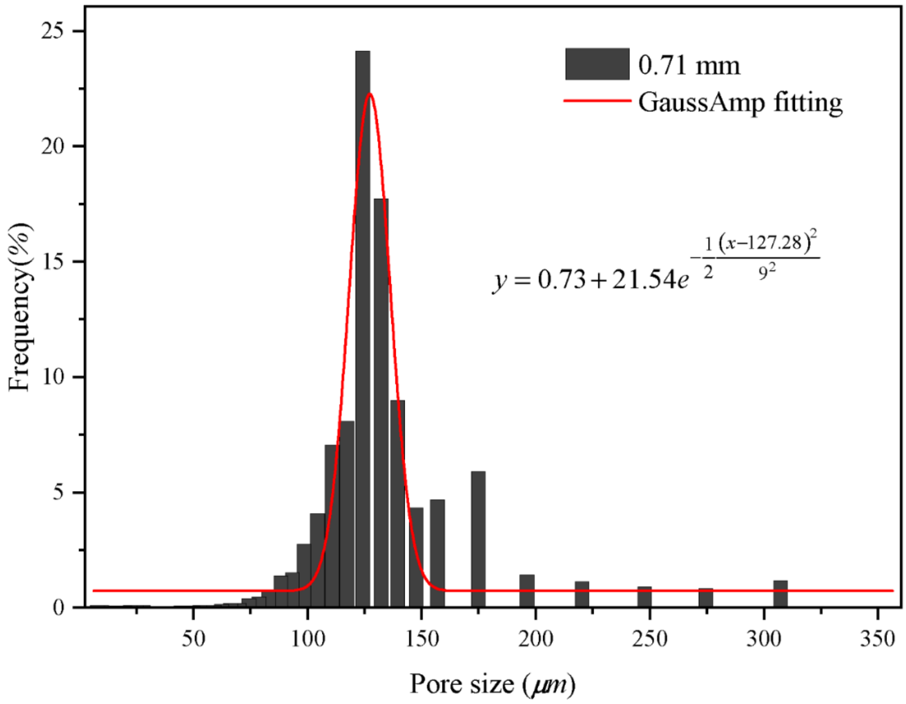

Figure 8. Histogram of pore size distribution of permeable stone with diameter of 0.71 mm.

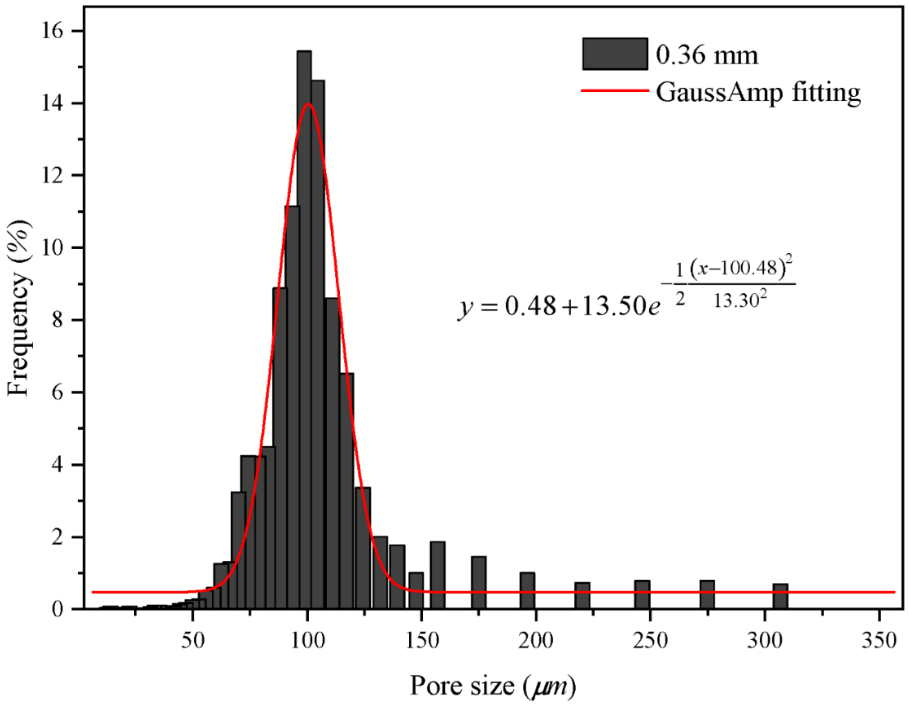

Figure 9. Histogram of pore size distribution of permeable stone with diameter of 0.36 mm.

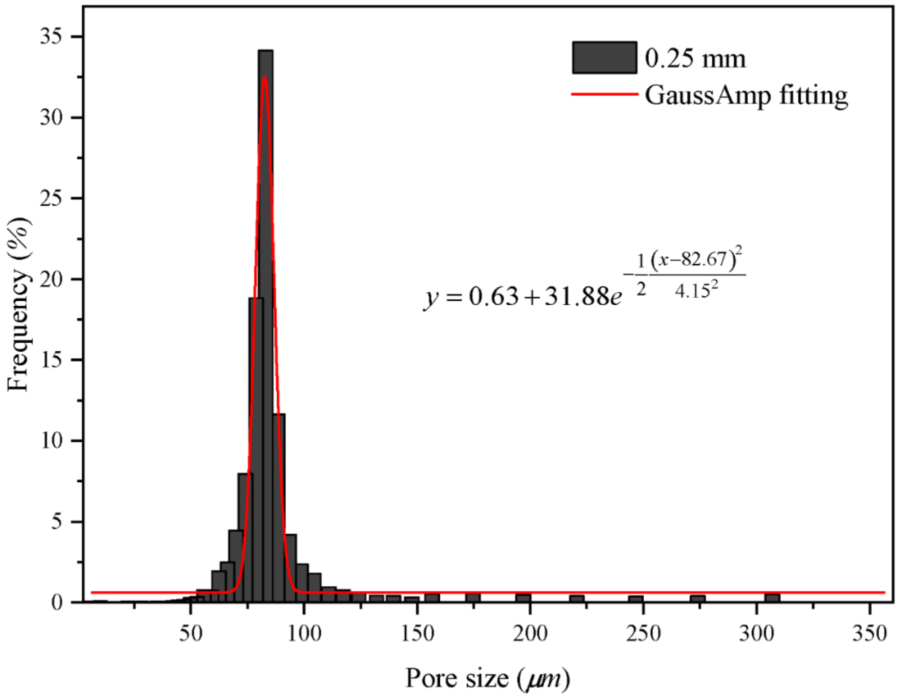

Figure 10. Histogram of pore size distribution of permeable stone with diameter of 0.25 mm.

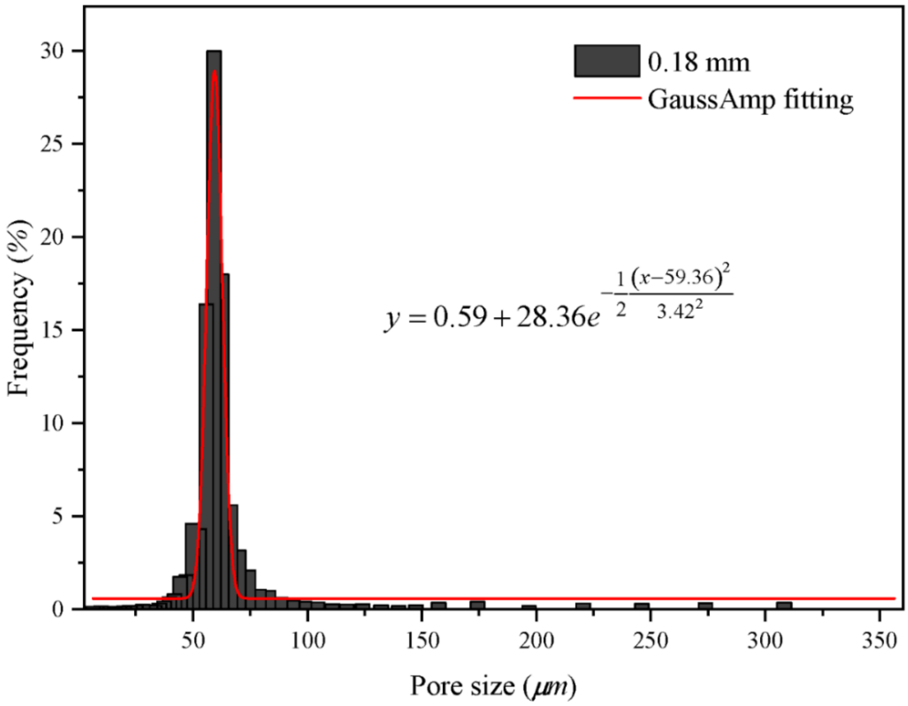

Figure 11. Histogram of pore size distribution of permeable stone with diameter of 0.18 mm.

From Fig. 8 to Fig. 11 we can find that the pore sizes of the four permeable stones are uniform and fall within narrow ranges. The pore size distributions of four different particle sizes show a skewed normal distribution. Besides, the pore maximum proportion (the peak of the curve, see Figs. 8-11) of permeable stones with different particle sizes are different, which are 124 μm, 99 μm, 83 μm and 59 μm, respectively. The Gaussian function is widely used to characterize the pore system and classify the petrophysical rock (Harlan et al., 1995; Jeon et al., 2014; Xu and Torres-Verdín, 2013), the general form of the Gauss function is shown below:

$$y = y_0 + He^{-\frac{(x-x_c)^2}{2w^2}} \tag{5}$$

where H is the height of the peak of the mercury injection curve, x_c is the abscissa corresponding to the peak of the curve (the pore size), w is the standard variance, which represents the width of the curve. To characterize the distribution of pore structure of four different permeable stones, we best-fit the Gaussian curve of the pore distribution of four permeable stones with different particle sizes, the best-fitted parameters are shown in Table 2. We can make several interesting observations from Table 2. Firstly, the expected value (x_c) decreases with decreasing particle sizes of permeable stone, the x_c values of different permeable stones are almost the same. Secondly, the standard variance (w) corresponding to the permeable stone of 0.18 mm is the smallest, indicating that the pore size distribution is more concentrated (or relatively homogeneous). For comparison, the pore size distribution of 0.36 mm permeable stone is the widest with the greatest variance. Finally, different values of H represent different proportions of pore sizes, among which the highest proportion can reach 34.04%. It will be desirable to establish a correlation between the parameters used in the pore-size distribution of Eq. (5) with the two Forchheimer coefficients A and B. This objective may be achieved using high-resolution pore-scale fluid mechanics simulations, which are out of the scope of this study. Further research is needed to address this issue in the future.

Table 2. Gaussian function characteristic values of four permeable stones with different particle sizes.

Mesh size	Particle size (mm)	y_0	H	x_c	w
24	0.71	0.73	21.54	127.28	9.00
46	0.36	0.48	13.49	100.48	13.30
60	0.25	0.63	31.88	82.67	4.15
80	0.18	0.59	28.36	59.36	3.42

The pore size distributions fall within ever narrower ranges with mesh sizes become larger. Moreover, the cumulative percentage frequency curves of the pore size distributions with different particle sizes are exhibited in Fig. 12 and the results are shown in Table 3.

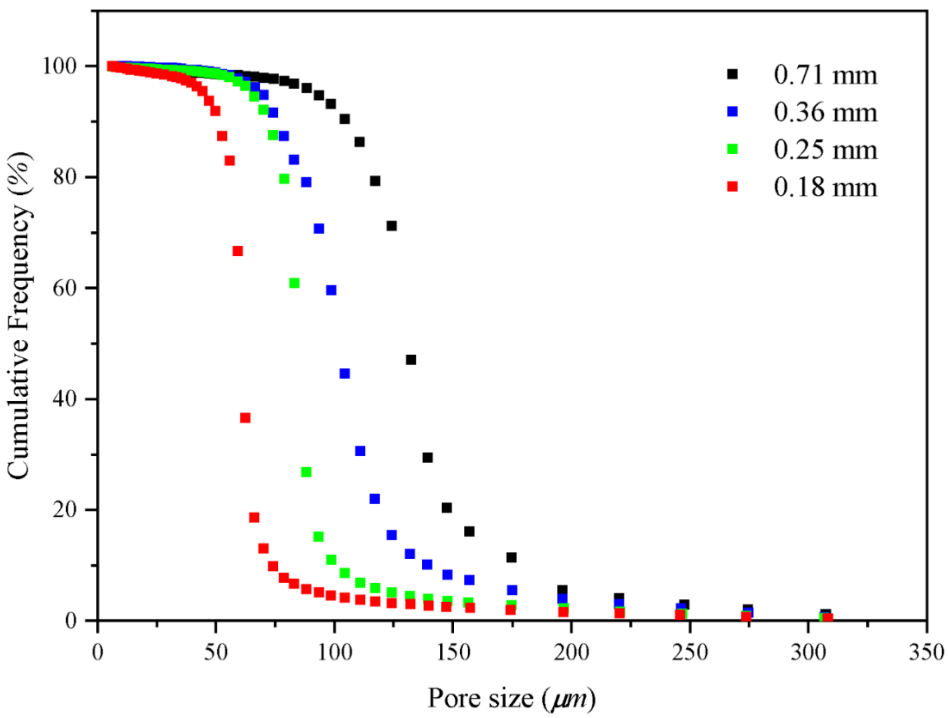

Figure 12. The cumulative frequency curve of pore size distribution.

Fig. 12 shows that D_{50} (the pore size corresponding to the median pressure P_{50}) increases with the increase of permeable stone particle size, the mean pore diameter (D_m) also increases.

In general, the pore size corresponding to the median pressure (denoted as D_{50}) may be slightly different than the mean pore diameter (D_m) which has been defined in different ways by various investigators when analyzing the pore size distributions (Hea and Zhangb, 2015; Zhen-Hua et al., 2007; Zhihong et al., 2000). As D_{50} is easily identifiable in the mercury injection experiments, it is used in this study as a representative of the mean pore diameter (D_m) of the permeable stone. Besides, the seepage law of permeable stone is closely related to the pore size, the smaller average pore size will result in a larger hydraulic gradient under the condition of the same specific discharge (see Fig. 4). The pore size characteristic values with different particle sizes are listed in Table 3. We find that the porosity decreases as the particle size increases while the mean pore diameter increases. The mean pore size can reflect the influence of particle diameter, sorting degree and arrangement mode of porous medium on seepage parameters.

Table 3. Pore size characteristic values of four permeable stones with different particle sizes.

Mesh size	Porosity (%)	D_m (μm)	D_{50} (μm)
24	32.35	131.31	131.34
46	36.69	102.56	103.42
60	40.82	84.73	85.09
80	42.88	60.97	61.12

Note: D_m is the mean pore diameter, D_{50} is the pore diameter corresponding to the median pressure P_{50}.

3.3 Analysis of influencing factors of Forchheimer equation coefficients

3.3.1 Influence of particle size on equation coefficient

The analysis of non-Darcy coefficient has always been of interest to many researchers working in different disciplines of porous media flow (Moutsopoulos et al., 2009; Sedghi-Asl et al., 2014; Shi et al., 2020). Different scholars have obtained a large amount of data through different experimental and simulation methods. They performed a quadratic fitting of the specific discharge and hydraulic gradient curves, developed numerous expressions for the Forchheimer coefficients. We obtained the coefficients of different fitting equations are shown in the following Table 4.

Table 4. The Forchheimer coefficients of empirical relations.

Equations	Coefficient A (sm^{-1})	Coefficient B (s^2m^{-2})
Ward (1964)	$A=\frac{360}{gd^2}$	$B=\frac{10.44}{gd}$
Blick (1966)	$A=\frac{32}{gnd^2}$	$B=\frac{C_D}{2gn^2d}$
Ergun (1952)	$A=\frac{150(1-n)^2}{gn^3d^2}$	$B=\frac{1.75(1-n)}{gn^3d}$
Macdonald et al. (1979)	$A=\frac{180(1-n)^2}{gn^{3.6}d^2}$	$B=\frac{1.8(1-n)}{gn^{3.6}d}$
Kovács (1981)	$A=\frac{144(1-n)^2}{gn^3d^2}$	$B=\frac{2.4(1-n)}{gn^3d}$
Kadlec and Knight (1996)	$A=\frac{255(1-n)^2}{gn^{3.7}d^2}$	$B=\frac{2(1-n)}{gn^3d}$
Irmay (1964)	$A=\frac{180(1-n)^2}{gn^3d^2}$	$B=\frac{0.6(1-n)}{gn^3d}$

Sidiropoulou et al. (2007) focused on the Forchheimer coefficients of porous media and evaluated the original theoretical equation above. The validity of these equations is verified using different experimental data. In addition, the Root Mean Square Error (RMSE) was used as a criterion to quantitatively evaluate the coefficients (Moutsopoulos et al., 2009). The different forms of Forchheimer coefficients described above are based on different assumptions and simplifications of pore structure. Consequently, these series of coefficients are applicable under specific conditions with different degrees of accuracy.

According to Eq. (2), the hydraulic gradient (J) is composed of a viscous force-related component (J_n) and an inertia force-related component (J_r), and for detailed discussion of this matter, one can refer to previous studies (Huang, 2012):

$$J_n = Aq = \frac{\alpha\mu}{\rho g}\frac{1}{d^2}q \quad J_r = \frac{\beta}{g}\frac{1}{d}q^2 \tag{6}$$

We can see from Eq. (6) that the J_n is inversely proportional to the square of the particle size, the J_r is inversely proportional to the particle size when the specific discharge remains the same. Both J_n and J_r are closely related to specific surface area and sizes of pores. As can be seen from the above analysis, the particle size is an important factor affecting the Forchheimer coefficient. Huang et al. (2013) carried out the seepage experiments in columns with different particle sizes, including 3mm, 5mm, 8mm and 10mm acrylic spheres. Accordingly, the coefficients A and B can be written as follows:

$$A = \frac{\alpha\mu}{\rho g}\frac{1}{d^2} \qquad B = \frac{\beta}{g}\frac{1}{d} \tag{7}$$

where α and β are constants related to the shape, sorting, and arrangement of the particles, and the specific derivation process is detailed in the previous study (Huang, 2012). The experimental results showed that the coefficient A was inversely proportional to the particle diameter square (d^2) and coefficient B was inversely proportional to the particle size (d) (Huang et al., 2013).

The uniform diameter cubic arrangement of porous media mentioned above is a rather ideal medium. The shape and arrangement of particles of natural pore aquifers are usually irregular. Therefore, the above-mentioned linear correlations between A and $1/d^2$, and between B and $1/d$ should be examined specifically. For this purpose, we collect the experimental data of homogeneous porous media, including the previous research results and the results of other scholars. Among them, samples P1-P4 are the permeable stones selected in this study, samples L1-L5 are from previous studies (Li et al., 2017), the experimental data of samples M1-M4 are from Moutsopoulos et al. (2009). The fitting coefficients are shown in Table 5. Furthermore, we can identify nice correlations between the Forchheimer coefficient *A* and $1/d^2$ and between the Forchheimer coefficient *B* and $1/d$, which are shown in Fig. 13 and Fig. 14, respectively.

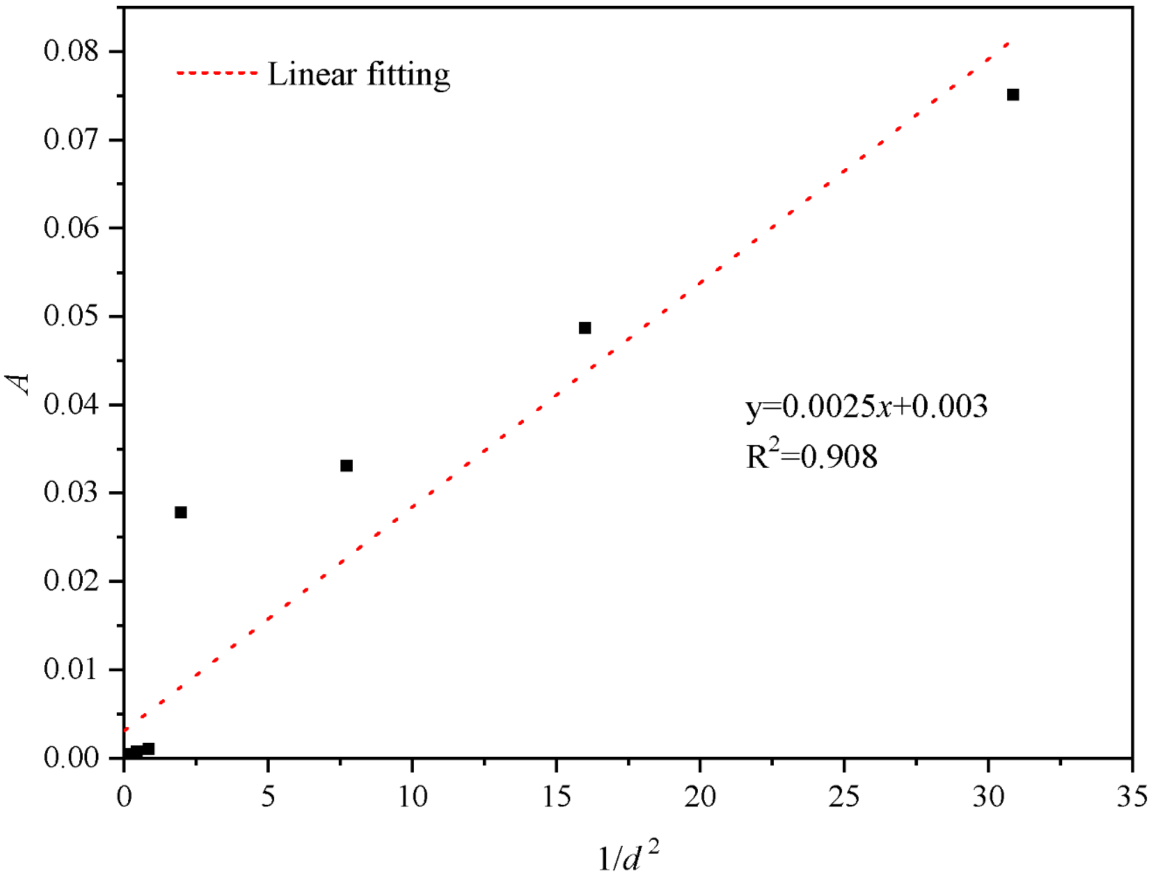

Figure 13. Variation of *A* with $1/d^2$ of different homogeneous particle sizes.

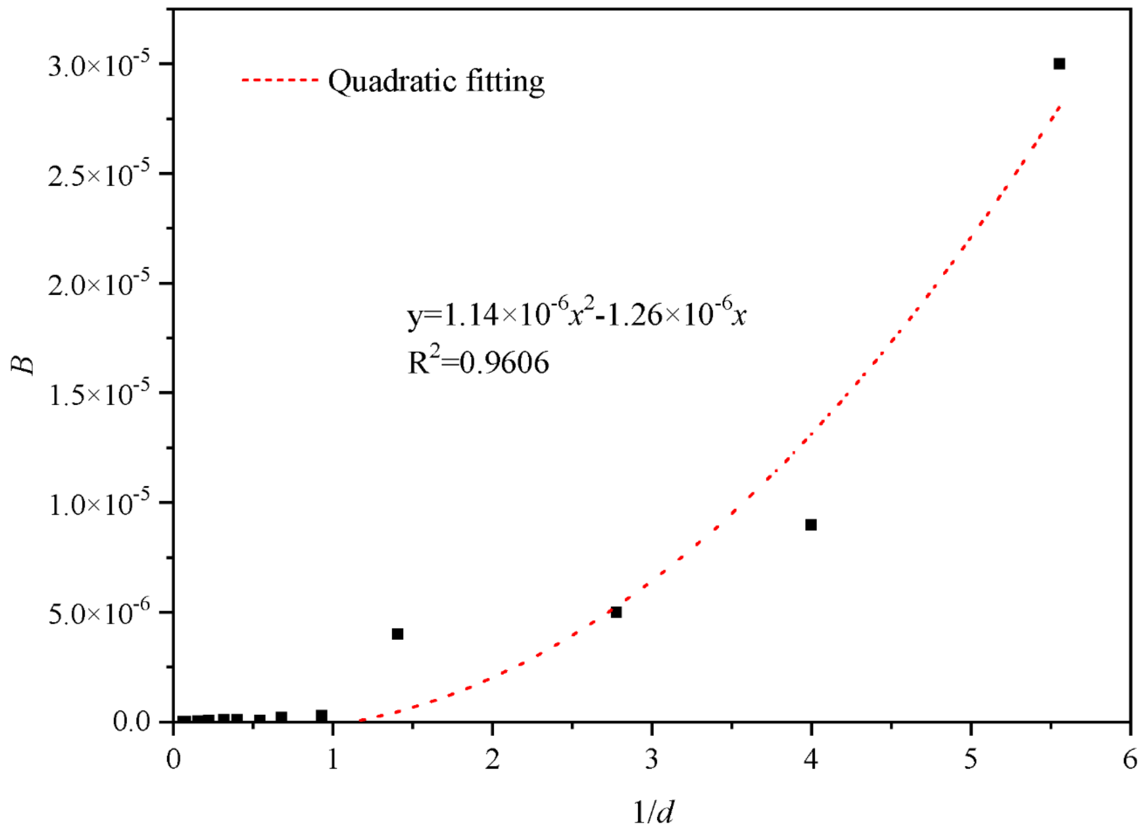

Figure 14. Variation of B with $1/d$ of different homogeneous particle sizes.

We can see from Fig. 13 that the coefficient A is linearly related to $1/d^2$ and the relationship between coefficient A and is given as $A = 0.0025\left(1/d^2\right) + 0.003$. The relationship between coefficient B and $1/d$ is completely different from the linear correlation as reported before. Fig. 14 shows that the coefficient B is quadratic related to $1/d$ and the relationship between coefficient B and $1/d$ is given as $B = 1.14\times10^{-6}\left(1/d\right)^2 - 1.26\times10^{-6}\left(1/d\right)$. The coefficients A and B show a linear relationship with $1/d^2$ and $1/d$ respectively when the particles are arranged in simple cube arrangement (Huang, 2012). That is to say, the irregular particles such as permeable stones have a more complex geometry, resulting in a different law from that of regular spherical particles. The structure of porous medium arranged in cubes is different from the permeable stone. The porosity of the porous media with spheres arranged in cubic is close to 0.48, independent of the diameter of spheres. While the particle shape, arrangement and tightness of permeable stone are different, and the porosity of permeable stone with different particle size is also different (see Table 3).

Table 5. Experimental fitting coefficient of different homogeneous particle sizes.

Sample	Particle size (mm)	Fitting equation	*A*	*B*	The correlation
P1	0.18	$y=0.0751x+3\times10^{-5}x^2$	0.0751	3×10^{-5}	0.9995
P2	0.25	$y=0.0487x+9\times10^{-6}x^2$	0.0487	9×10^{-6}	0.9998
P3	0.36	$y=0.0331x+5\times10^{-6}x^2$	0.0331	5×10^{-6}	1
P4	0.71	$y=0.0278x+4\times10^{-6}x^2$	0.0278	4×10^{-6}	0.9995
L1	1.075	$y=0.001x+3\times10^{-7}x^2$	0.001	3×10^{-7}	0.9999
L2	1.475	$y=0.0007x+2\times10^{-7}x^2$	0.0007	2×10^{-7}	0.9998
L3	1.85	$y=0.0005x+5\times10^{-8}x^2$	0.0005	5×10^{-8}	0.9998
L4	2.5	$y=0.0005x+9\times10^{-8}x^2$	0.0005	9×10^{-8}	0.9997
L5	3.17	$y=0.0004x+1\times10^{-7}x^2$	0.0004	1×10^{-7}	0.9998
M1	4.5	$y=3\times10^{-5}x+7\times10^{-8}x^2$	3×10^{-5}	7×10^{-8}	0.9913
M2	6.39	$y=3\times10^{-5}x+3\times10^{-8}x^2$	3×10^{-5}	3×10^{-8}	0.9984
M3	12.84	$y=1\times10^{-5}x+2\times10^{-8}x^2$	1×10^{-5}	2×10^{-8}	0.9977
M4	16	$y=1\times10^{-5}x+2\times10^{-8}x^2$	1×10^{-5}	2×10^{-8}	0.998

3.3.2 Influence of porosity on equation coefficient

In above sections, we have analyzed the influence of particle sizes on seepage coefficient. Furthermore, the pore size and pore specific surface area are also related to the arrangement and sorting degree of particles, that is, to the porosity of porous media. To explore the effect of sorting degree on seepage coefficient, we draw a schematic diagram of different sorting degree of particles, as shown in Fig. 15 (a) and (b). The degree of particle sorting is one of the important factors affecting the pore size. In porous media with a poor sorting degree, the pore size is usually determined by the diameter of the smallest particle. We can see from Fig. 15 that the pores between the larger particles are filled by smaller particles, resulting in even smaller pores. In addition, the poorer sorting degree of particles leads to the larger pore specific surface area and stronger viscous force of flow, which can lead to a larger coefficient *A*.

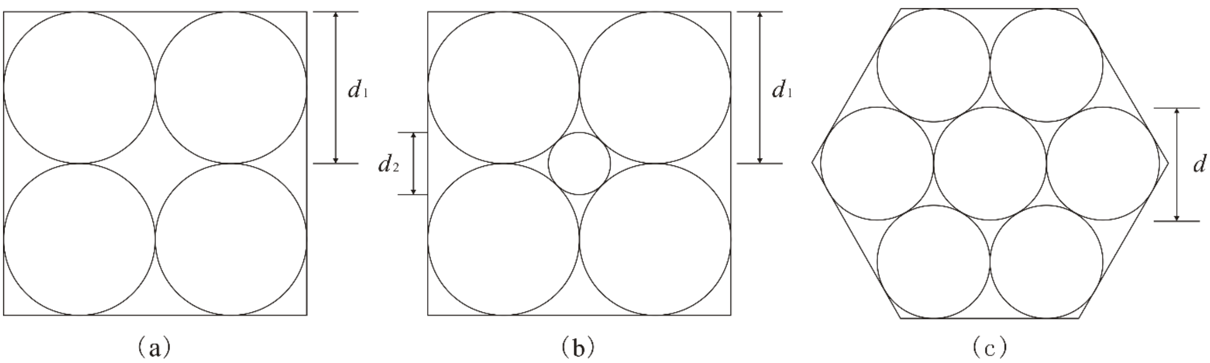

Figure 15. The schematic diagram of different particle sizes and arrangements in (a) a cubic arrangement with identical solid grains; (b) a cubic arrangement with two different sizes of solid grains; (c) a hexahedron arrangement with identical solid grains. d_1 is the diameter of (identical) solid grains in (a) and the diameter of the larger solid grains in (b), d_2 is the diameter of the smaller solid grain in (b), d is the diameter of the (identical) solid grains in (c).

Furthermore, we have also provided the schematic diagrams of spherical particles with equal size in two simple arrangements, namely cubic arrangement and hexahedron arrangement, as shown in Fig. 15 (a) and (c). The cube arrangement is the less compact arrangement with a pore diameter of $0.414d_1$, while the hexahedron arrangement is the more compact arrangement with a pore diameter of 0.155d, where d_1 and d have been explained in the caption of Fig. 15. The characteristic value of pore structure in different arrangement with the same particle size are shown in Table 6. We can see that different arrangement modes will substantially affect the pore specific surface area and pore size of porous media. The more compactly packed particles lead to the larger pore specific surface area and stronger viscous force. Meanwhile, the smaller pore diameter is associated with stronger effect of viscous force and inertia force. In summary, the better sorting degree of particles leads to the weaker viscous and inertial forces, then the coefficients A and B will be smaller. As the better sorting degree and the less compact (or looser) arrangement particles mean the larger porosity, so we can conclude that the larger porosity leads to the smaller coefficients A and B under the condition of the same particle size.

Table 6. Characteristic value of pore structure in different arrangement with the same particle size.

Arrangement mode	Side length	Porosity (%)	Specific surface area
Cube	2d	47.60	3.142
Hexahedron	1.577d	43.30	3.402

However, the structure of natural porous media is much more complex and heterogeneous than what has been shown in Figure 15, so it is difficult to quantitatively describe the effect of sorting degree and arrangement on seepage law.

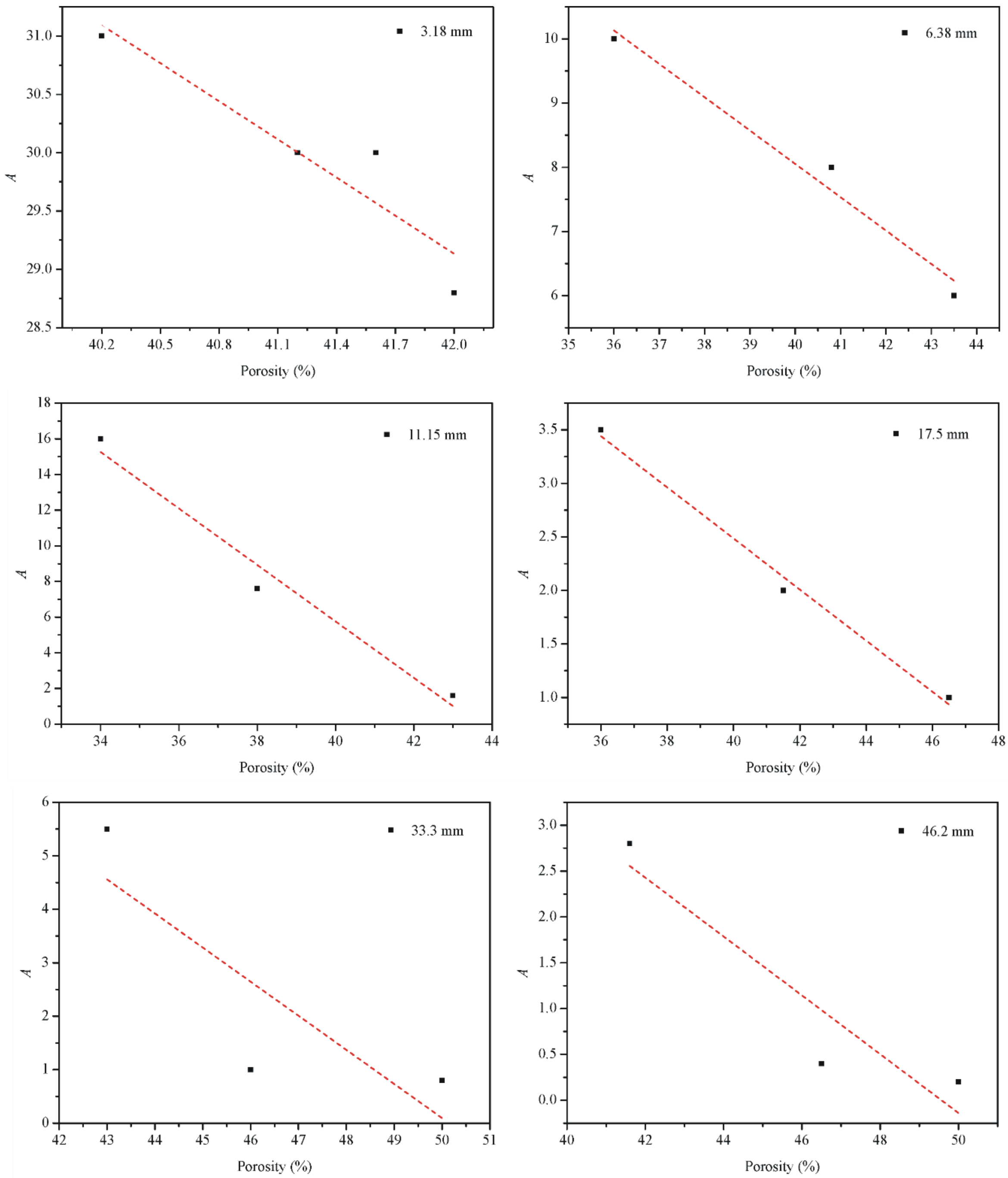

Figure 16. Variation of *A* with *n* of six gravels with different particle sizes.

In view of this, we can use a macro parameter porosity (n) to reveal the effect of sorting degree and arrangement on seepage coefficient. In order to verify the correctness of the above analysis results, we selected the seepage experiment results of Niranjan (1973) for further validation. Niranjan (1973) chose gravel of the same size but different porosity and carried out seepage experiments. We selected the experimental results of six different particle sizes with 3.18 mm, 6.38 mm, 11.15 mm, 17.5 mm, 33.3 mm and 46.2 mm from Niranjan (1973), and drew the relationship between coefficient *A* and *B* and porosity respectively, as shown in Fig. 16 and Fig. 17. We can see that the coefficients *A* and *B* of the six groups of experimental data of Niranjan (1973) decrease with the increase of porosity, which is consistent with our theoretical analysis of this investigation.

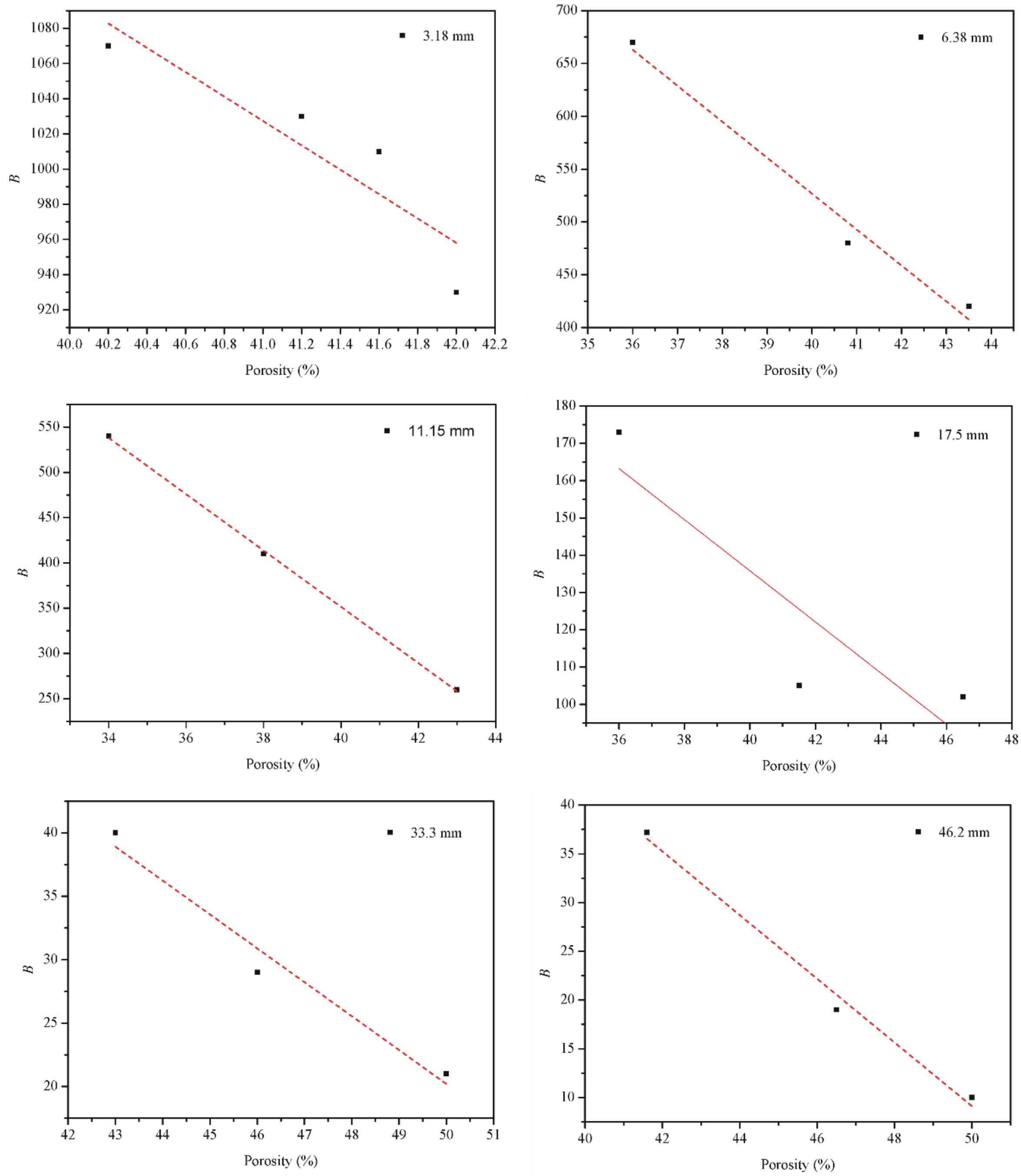

Figure 17. Variation of *B* with *n* of six gravels with different particle sizes.

4. Summary and conclusions

This study presents experimental results of Forchheimer flow in four different permeable stones with different mesh sizes, including 24 mesh size (0.71 mm), 46 mesh size (0.36 mm), 60 mesh size (0.25 mm), 80 mesh size (0.18 mm). The effects of mean pore size and pore size distribution on the transition of flow regimes (from pre-Darcy to post-Darcy) are discussed. In addition, the mercury injection technique is proposed to investigate the pore distribution of the permeable stones. Beyond that, the Forchheimer coefficients are specifically discussed. The main conclusions can be summarized as follows:

1) The relationships between specific discharge (q) and the “pseudo” hydraulic conductivity (K) (which is computed as a ratio of q and the hydraulic gradient, J) of permeable stones show that deviation from Darcy flow regime is clearly visible. In addition, the critical specific discharge corresponding to the transition of flow regimes (from pre-Darcy to post-Darcy) increases with the increase of mean particle size.

2) When the specific discharge is small, only a small fraction of the pore water flowing through the pores. The rest of the pore water adheres to the surface of the solid particles (immobile), partially blocking the flow pathways. As the specific discharge increases, more pore water becomes mobile and participates in flow. Hence, the "pseudo" hydraulic conductivity increases with the increase of specific discharge. When the specific discharge increases to the critical specific discharge (q_c), the "pseudo" hydraulic conductivity is maximized, and then it begins to decrease as the specific discharge continues to increase.

3) The mercury injection experiment results show that the mercury injection curve can be divided into three segments. The beginning and end segments of the mercury injection curve of the four permeable stones with different particle sizes are very gentle, while the main (or intermediate) mercury injection curve is steep, indicating that the pore size distribution falls within a narrow range, the proportions of large pores and small pores are relatively small.

4) The porosity decreases as the mean particle size of permeable stone increases while the mean pore diameter increases. The porosity can reflect the influence of particle diameter, sorting degree and arrangement mode of porous medium on seepage parameters. A larger porosity leads to smaller coefficients *A* and *B* under the condition of the same particle size.

5) The coefficient *A* is linearly related to $1/d^2$ and the relationship between coefficient *A* and $1/d^2$ is given as $A = 0.0025\left(1/d^2\right) + 0.003$. The coefficient *B* is not linearly related to $1/d$, instead it is quadratic related to $1/d$ as $B = 1.14\times10^{-6}\left(1/d\right)^2 - 1.26\times10^{-6}\left(1/d\right)$. The particle shape and arrangement of permeable stone have imposed great influences on the seepage parameters.

Notation

q	The specific discharge, md^{-1}.
K	The “pseudo” hydraulic conductivity, md^{-1}.
J	The hydraulic gradient.
A	The Forchheimer equation coefficient (viscous force item), sm^{-1}.
B	The Forchheimer equation coefficient (Inertia force item), s^2m^{-2}.
a, b	The empirical parameters depend on materials properties.
Re	The Reynold number.
Re_c	The critical Reynold number.
M, m	The coefficients determined by fluid and properties.
C_D	The appropriate phenomenological coefficient.
P_c	The capillary force, *Pa*.
P_{50}	The corresponding pressure value when the saturation reaches 50%, *MPa*.

P_A, P_B, P_C The pressure corresponding to different stages on mercury injection curve, *MPa*.

σ The solid-liquid interfacial tension, Nm^{-1}.

θ The wet angle between the liquid and the solid surface.

r The radius of curvature in capillary, *mm*.

d The particle size, *mm*.

d_{50} The mean particle sizes (50% by weight), *mm*.

D_m The mean pore diameter, μm.

D_{50} The pore diameter corresponding to the median pressure P_{50}, μm.

H The height of the peak of the mercury injection curve.

x_c The abscissa corresponding to the peak of the curve (the pore size).

w The standard variance.

n The porosity.

J_n The viscous force-related component.

J_r The inertia force-related component.

Authors contributions

Zhongxia Li: Experiment, Writing original draft. Junwei Wan: Methodology, Conceptualization. Tao Xiong: Data curation, Investigation, Experiment. Hongbin Zhan: Methodology, Writing, Review & Editing. Linqing He: Experiment, Methodology. Kun Huang: Funding acquisition, Investigation

Competing interests

The authors declare that they have no conflict of interest.

Acknowledgements

This study was supported by the National Natural Science Foundation of China (Grant Nos. 41402204), the National Key Research and Development Program of China (No. 2018YFC0604202) and the Fundamental Research Funds for National Universities, China University of Geosciences (Wuhan). Thank Zhongzhi Shen of China University of Geosciences for his great help in developing the experimental set up. The authors want to express their sincere appreciation of the constructive comments made by the two anonymous reviewers and Associate Editor for improving the quality of the manuscript.

References

Alvarez, A. E., Mahmoud, E., Martin, A. E., Masad, E., and Estakhri, C.: Stone-on-stone contact of permeable friction course mixtures, Journal of Materials in Civil Engineering, 22, 1129-1138, https://doi.org/10.1061/(ASCE)MT.1943-5533.0000117, 2010.

Anovitz, L. M. and Cole, D. R.: Characterization and Analysis of Porosity and Pore Structures, Reviews in Mineralogy and Geochemistry, 80, 61-164, https://doi.org/10.2138/rmg.2015.80.04, 2015.

Bear, J.: Dynamics of Fluids in Porous Media, American Elsevier Pub. Co., New York, N.Y., and Amsterdam,1972.

Beavers, G. S., Sparrow, E., and Rodenz, D. E.: Influence of Bed Size on the Flow Characteristics and Porosity of Randomly Packed Beds of Spheres, Journal of Applied Mechanics, 40, 655-660, https://doi.org/10.1115/1.3423067, 1972.

Blick, E.: Capillary-Orifice Model for High-Speed Flow through Porous Media, Industrial Engineering Chemistry Process Design Development, 5, 90-94, https://doi.org/10.1021/i260017a019, 1966.

Bu, S., Yang, J., Dong, Q., and Wang, Q.: Experimental study of transition flow in packed beds of spheres with different particle sizes based on electrochemical microelectrodes measurement, Applied Thermal Engineering, 73, 1525-1532, 2014.

Darcy, H.: Recherches expérimentales relatives au mouvement de l'eau dans les tuyaux, Impr. Impériale, Paris, France,1857.

Dejam, M., Hassanzadeh, H., and Chen, Z.: Pre-Darcy flow in porous media, Water Resources Research, 53, 8187-8210, https://doi.org/10.1002/2017WR021257, 2017.

Dudgeon, C. R.: An experimental study of the flow of water through coarse granular media, La Houille Blanche, 785-801, https://doi.org/10.1051/lhb/1966049, 1966.

Dybbs, A. and Edwards, R.: A new look at porous media fluid mechanics—Darcy to turbulent, in: Fundamentals of transport phenomena in porous media, Springer, 199-256, 1984.

Ergun, S.: Fluid flow through packed columns, Chemical Engineering Progress, 89-94, https://doi.org/10.1016/0009-2509(53)80048-5, 1952.

Fancher, G. H. and Lewis, J. A.: Flow of simple fluids through porous materials, Industrial & Engineering

Chemistry, 25, 1139-1147, https://doi.org/10.1021/ie50286a020, 1933.

Fetter, C. W.: Applied Hydrogeology:International Edition, Prentice Hall, Pearson, Engelwood Cliffs,2001.

Forchheimer, P.: Wasserbewegung durch boden, Z. Ver. Deutsch, Ing., 45, 1728-1782, 1901.

Geertsma, J.: Estimating the Coefficient of Inertial Resistance in Fluid Flow Through Porous Media, Society of Petroleum Engineers Journal, 14, 445-450, https://doi.org/10.2118/4706-PA, 1974.

Guan, X., Wang, J., and Xiao, F.: Sponge city strategy and application of pavement materials in sponge city, Journal of Cleaner Production, 127022, https://doi.org/10.1016/j.jclepro.2021.127022, 2021.

Hall, P. L., Mildner, D., and Borst, R. L.: Small-angle scattering studies of the pore spaces of shaly rocks, Journal of Geophysical Research Atmospheres, 91, 2183-2192, https://doi.org/10.1029/JB091iB02p02183, 1986.

Han, D., Wei, L., and Zhang, J.: Experimental study on performance of asphalt mixture designed by different method, Procedia engineering, 137, 407-414, https://doi.org/10.1016/j.proeng.2016.01.275, 2016.

Harlan, J., Picot, D., Loll, P., and Garavito, R.: Calibration of size-exclusion chromatography: use of a double Gaussian distribution function to describe pore sizes, Analytical biochemistry, 224, 557-563, https://doi.org/10.1006/abio.1995.1087, 1995.

Hea, X. and Zhangb, Z.: Microscopic Pore Structural Characteristics in Coal Particles, International Conference on Material, Guangzhou, China,

Huang, K.: Exploration of the basic seepage equation in porous media, PhD dissertation, 2012.

Huang, K., Wan, J., Chen, C., Linqing, H., Mei, W., and Zhang, M.: Experimental investigation on water flow in cubic arrays of spheres, Journal of Hydrology, 492, 61-68, https://doi.org/10.1016/j.jhydrol.2013.03.039, 2013.

Irmay, S.: Theoretical models of flow through porous media, RILEM Symp. Transfer of Water in porous media, Paris, Bull. RILEM, 29, 37-43, 1964.

Izbash, S.: O Filtracii V Kropnozernstom Materiale, Leningrad, USSR, 1931.

Javadi, M., Sharifzadeh, M., Shahriar, K., and Mitani, Y.: Critical Reynolds number for nonlinear flow through rougˆ walled fractures: The role of shear processes, Water Resources Research, 50, 1789-1804, https://doi.org/10.1002/2013WR014610, 2014.

Jeon, H., Cho, H., Kim, J., and Sung, B.: Non-Gaussian rotational diffusion in heterogeneous media, Physical Review E Statistical Nonlinear & Soft Matter Physics, 90, 042105, https://doi.org/10.1103/PhysRevE.90.042105, 2014.

Kadlec, R. H. and Knight, R. L.: Treatment Wetlands, Lewis Pub, Boca Raton,1996.

Kate, J. M. and Gokhale, C. S.: A simple method to estimate complete pore size distribution of rocks, Engineering Geology, 84, 48-69, https://doi.org/10.1016/j.enggeo.2005.11.009, 2006.

Koch, D. and Ladd, A.: Moderate Reynolds number flows through periodic and random arrays of aligned cylinders, Journal of Fluid Mechanics, 349, 31-66, https://doi.org/10.1017/S002211209700671X, 1996.

Kovács, G.: Seepage Hydraulics, Development in Water Sciences. Elsevier: New York, 1981.

Latifi, M., Midoux, N., Storck, A., and Gence, J.: The use of micro-electrodes in the study of the flow regimes in a packed bed reactor with single phase liquid flow, Chemical engineering science, 44, 2501-2508, 1989.

Li, Q., Wang, F., Yu, Y., Huang, Z., Li, M., and Guan, Y. J. J. o. E. M.: Comprehensive performance evaluation of LID practices for the sponge city construction: a case study in Guangxi, China, Journal of Environmental Management, 231, 10-20, https://doi.org/10.1016/j.jenvman.2018.10.024, 2019a.

Li, Z., Wan, J., Huang, K., Chang, W., and He, Y.: Effects of particle diameter on flow characteristics in sand columns, International Journal of Heat & Mass Transfer, 104, 533-536, https://doi.org/10.1016/j.ijheatmasstransfer.2016.08.085, 2017.

Li, Z., Wan, J., Zhan, H., Cheng, X., Chang, W., and Huang, K.: Particle size distribution on Forchheimer flow and transition of flow regimes in porous media, Journal of Hydrology, 574, 1-11, https://doi.org/10.1016/j.jhydrol.2019.04.026, 2019b.

Lindquist, E.: On the flow of water through porous soil, Premier Congres des grands barrages (Stockholm)1933.

Lindquist, W. B., Venkatarangan, A., Dunsmuir, J., and Wong, T. F.: Pore and throat size distributions measured from synchrotron X-ray tomographic images of Fontainebleau sandstones, Journal of Geophysical Research Solid Earth, 105, 21509-21527, https://doi.org/10.1029/2000JB900208, 2000.

Maalal, O., Prat, M., Peinador, R., and Lasseux, D.: Determination of the throat size distribution of a porous medium as an inverse optimization problem combining pore network modeling and genetic and hill climbing algorithms, Physical Review E, 103, 023303, https://doi.org/10.1103/PhysRevE.103.023303, 2021.

Macdonald, I., El-Sayed, M., Mow, K., and Dullien, F.: Flow through porous media-the Ergun equation revisited, Industrial & Engineering Chemistry Fundamentals, 18, 199-208, https://doi.org/10.1021/i160071a001, 1979.

Moutsopoulos, K. N., Papaspyros, I. N., and Tsihrintzis, V. A.: Experimental investigation of inertial flow processes in porous media, Journal of hydrology, 374, 242-254, https://doi.org/10.1016/j.jhydrol.2009.06.015, 2009.

Niranjan, H.: Non-Darcy flow through porous media, M.S., dissertation, ITT, Kanpur, India, 1973.

Panfilov, M. and Fourar, M.: Physical splitting of nonlinear effects in high-velocity stable flow through porous media, Advances in Water Resources, 29, 30-41, https://doi.org/10.1016/j.advwatres.2005.05.002, 2006.

Pittman, E. D.: Relationship of porosity and permeability to various parameters derived from mercury injection-capillary pressure curves for sandstone (1), AAPG bulletin, 76, 191-198, https://doi.org/10.1306/BDFF87A4-1718-11D7-8645000102C1865D, 1992.

Prowell, B. D., Allen Cooley Jr, L., and Schreck, R. J.: Virginia's experience with 9.5-mm nominal-maximum-aggregate-size stone matrix asphalt, Transportation research record, 1813, 133-141, https://doi.org/10.3141/1813-16, 2002.

Rezaee, R., Saeedi, A., and Clennell, B.: Tight gas sands permeability estimation from mercury injection capillary pressure and nuclear magnetic resonance data, Journal of Petroleum Science and Engineering, 88, 92-99, https://doi.org/10.1016/j.petrol.2011.12.014, 2012.

Rijfkogel, L. S., Ghanbarian, B., Hu, Q., and Liu, H. H.: Clarifying pore diameter, pore width, and their relationship through pressure measurements: A critical study, Marine and Petroleum Geology, 107, 142-148, https://doi.org/10.1016/j.marpetgeo.2019.05.019, 2019.

Scheidegger, A.: The physics of flow through porous media,

Scheidegger, A. E.: On the stability of displacement fronts in porous media: a disscussion of the muskat-aronofsky model, Canadian Journal of Physics, 38, 153-162, https://doi.org/10.1139/p60-017, 1960.

Scheidegger, A. E.: The physics of flow through porous media, University of Toronto Press, https://doi.org/10.3138/9781487583750, 2020.

Schmitt, M., Fernandes, C. P., da Cunha Neto, J. A., Wolf, F. G., and dos Santos, V. S.: Characterization of pore systems in seal rocks using nitrogen gas adsorption combined with mercury injection capillary pressure techniques, Marine and Petroleum Geology, 39, 138-149, https://doi.org/10.1016/j.marpetgeo.2012.09.001, 2013.

Schneebeli, G.: Experiences sur la limite de validite de la loi de Darcy et l'apparition de la turbulence dans un ecoulemant de filtration, La Huille Blanche, 2, 141-149, https://doi.org/10.1051/lhb/1955030, 1955.

Sedghi-Asl, M., Rahimi, H., and Salehi, R.: Non-Darcy Flow of Water Through a Packed Column Test, Transport in Porous Media, 101, 215-227, https://doi.org/10.1007/s11242-013-0240-0, 2014.

Seguin, D., Montillet, A., Comiti, J., and Huet, F.: Experimental characterization of flow regimes in various porous media—II: Transition to turbulent regime, Chemical engineering science, 53, 3897-3909, 1998.

Shi, W., Yang, T., and Yu, S.: Experimental Investigation on Non-Darcy Flow Behavior of Granular Limestone with Different Porosity, Journal of Hydrologic Engineering, 25, 06020004, https://doi.org/10.1061/(ASCE)HE.1943-5584.0001966, 2020.

Sidiropoulou, M. G., Moutsopoulos, K. N., and Tsihrintzis, V.: Determination of Forchheimer equation coefficients a and b, Hydrological Processes, 21, 534-554, https://doi.org/10.1002/hyp.6264, 2007.

Skjetne, E., Hansen, A., and Gudmundsson, J.: High-velocity flow in a rough fracture, Journal of Fluid Mechanics, 383, 1-28, https://doi.org/10.1017/S0022112098002444, 1999.

Soni, J., Islam, N., and Basak, P.: An experimental evaluation of non-Darcian flow in porous media, Journal of Hydrology, 38, 231-241, https://doi.org/10.1016/0022-1694(78)90070-7, 1978.

Souto, H. P. A. and Moyne, C.: Dispersion in two-dimensional periodic porous media. Part I. Hydrodynamics, Physics of Fluids, 9, 2243-2252, https://doi.org/10.1063/1.869365, 1997.

Suo, Z., Bao, X., Nie, L., Yan, Q., and Qi, K.: Optimization Design of Mix Proportion of Large Stone Permeable Mixture Based on Target Air Voids, Buildings, 11, 514, https://doi.org/10.3390/buildings11110514, 2021.

Swartzendruber, D.: Modification of Darcy's law for the flow of water in soils, Soil Science, 93, 22-29, https://doi.org/10.1097/00010694-196201000-00005, 1962a.

Swartzendruber, D.: Non‐Darcy flow behavior in liquid‐saturated porous media, Journal of Geophysical Research, 67, 5205-5213, https://doi.org/10.1029/JZ067i013p05205, 1962b.

Van Lopik, J. H., Zazai, L., Hartog, N., and Schotting, R.: Nonlinear Flow Behavior in Packed Beds of Natural and Variably Graded Granular Materials, Transport in Porous Media, 131, 957-983, https://doi.org/10.1007/s11242-019-01373-0, 2019.

Van Lopik, J. H., Snoeijers, R., van Dooren, T. C. G. W., Raoof, A., and Schotting, R. J.: The Effect of Grain Size Distribution on Nonlinear Flow Behavior in Sandy Porous Media, Transport in Porous Media, 120, 1-30, https://doi.org/10.1007/s11242-017-0903-3, 2017.

Wang, J., Ng, P.-L., Gong, Y., Su, H., and Du, J.: Experimental Study of Low Temperature Performance of Porous Asphalt Mixture, Applied Sciences, 11, 4029, https://doi.org/10.3390/app11094029, 2021.

Ward, J. C.: Turbulent Flow in Porous Media, Journal of Hydraulic Engineering, 90, 1-12, http://dx.doi.org/10.1016/S0301-9322(02)00051-4, 1964.

Washburn, E. W.: The Dynamics of Capillary Flow, Physical Review, 17, 273-283, https://doi.org/10.1103/PhysRev.17.273, 1921.

Wright, D.: Nonlinear Flow Through Granular Media, Journal of Hydraulic Engineering, 94, 851-872, https://doi.org/10.1061/JYCEAJ.0001858, 1968.

Xie, H. and Watson, D. E.: Determining air voids content of compacted stone matrix asphalt mixtures, Transportation research record, 1891, 203-211, https://doi.org/10.3141/1891-24, 2004.

Xu, C. and Torres-Verdín, C.: Pore System Characterization and Petrophysical Rock Classification Using a Bimodal Gaussian Density Function, Mathematical Geosciences, 45, 753-771, https://doi.org/10.1007/s11004-013-9473-2, 2013.

Yang, B., Yang, T., Xu, Z., Liu, H., Yang, X., and Shi, W.: Impact of Particle-Size Distribution on Flow Properties of a Packed Column, Journal of Hydrologic Engineering, 24, 04018070, https://doi.org/10.1061/(ASCE)HE.1943-5584.0001735, 2019.

Yu, T., Liu, D., Zhang, H., and Wang, H.: Influence of pore water phase change on service performance for permeable pavement in Sponge City, Water Science and Technology, 84, 3769-3779, https://doi.org/10.2166/wst.2021.459, 2021.

Zeng, Z. and Grigg, R.: A criterion for non-Darcy flow in porous media, Transport in porous media, 63, 57-69, https://doi.org/10.1007/s11242-005-2720-3, 2006.

Zhen-hua, MIN, and, Min, CAO, and, Shu, ZHANG, and, and Xiu-dan: Effect of precursor on the pore structure of carbon foams, New Carbon Materials, 22, 75-79, https://doi.org/10.1016/S1872-5805(07)60009-2, 2007.

Zhihong, L. I., Jihong, S., Dong, W. U., Yuhan, S., Liu, Y. I., Wenjun, S., and Baozhong, D.: Determination of average pore diameter of SiO2 xerogels by small angle X-ray scattering, ACTA Physica sinica, 49, 1312-1315, https://doi.org/10.3321/j.issn:1000-3290.2000.07.020, 2000.

Zhou, H., Fang, Y.-g., Chen, M., Gu, R.-g., and Li, W.: Experimental and analytical study on electro-osmosis in low-permeability soil considering the pore size effect, Geotechnique, 71, 141-152, https://doi.org/10.1680/jgeot.18.p.362, 2019.